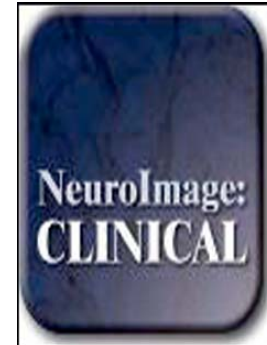Accepted Manuscript

Motor pathway degeneration in young ataxia telangiectasia patients: A diffusion tractography study

Ishani Sahama, Kate Sinclair, Simona Fiori, James Doecke, Kerstin Pannek, Lee Reid, Martin Lavin, Stephen Rose

Please cite this article as: Sahama, Ishani, Sinclair, Kate, Fiori, Simona, Doecke, James, Pannek, Kerstin, Reid, Lee, Lavin, Martin, Rose, Stephen, Motor pathway degeneration in young ataxia telangiectasia patients: A diffusion tractography study, *NeuroImage: Clinical* (2015), doi: 10.1016/j.nicl.2015.08.007

This is a PDF file of an unedited manuscript that has been accepted for publication. As a service to our customers we are providing this early version of the manuscript. The manuscript will undergo copyediting, typesetting, and review of the resulting proof before it is published in its final form. Please note that during the production process errors may be discovered which could affect the content, and all legal disclaimers that apply to the journal pertain.

Motor pathway degeneration in young ataxia telangiectasia patients: A diffusion tractography study

Ishani Sahama, BSc Hons.[a], Kate Sinclair, MD[b], Simona Fiori, MD[c], James Doecke, PhD[d],

Kerstin Pannek, PhD[e], Lee Reid, MSc[d], Martin Lavin, PhD[f], Stephen Rose, PhD[d]

[a]The University of Queensland, School of Medicine, Brisbane, Australia

[b]Neurology, The Royal Children's Hospital, Brisbane, Australia

[c]IRCCS Stella Maris, Calambrone, Pisa, Italy

[d]Digital Productivity Flagship/ The Australian e-Health Research Centre, Commonwealth

Scientific and Industrial Research Organization, Brisbane, Australia

[e]Imperial College London, London, United Kingdom

[f]University of Queensland Centre for Clinical Research, Brisbane, Australia

Corresponding author

A/Prof Stephen E Rose

CSIRO Centre for Computational Informatics

Level 5, UQ Health Sciences Building, RBWH

Herston 4029

Australia

Phone: +61 7 3253 3620

Email: Stephen.Rose@csiro.au

Word count:

Abstract (with headings and abbreviations): 241 words

Body (with in-text references and figure legends): 5118 words

Keywords: Ataxia Telangiectasia, Cerebellum, Diffusion Magnetic Resonance Imaging,

Whole Tract Statistics.

Running title: White Matter Tracts in Ataxia Telangiectasia.

Highlights

- Corticomotor and corticospinal ataxia telangiectasia patient tracts were analyzed

- Decreases in fractional anisotropy occurred along patient tracts

- Mean diffusivity was reduced in cerebellar peduncles in patients

- Patient corticospinal streamline number and apparent fiber density was reduced

- Young ataxia telangiectasia patients show advanced white matter degeneration

Abstract

Background: Our understanding of the effect of ataxia-telangiectasia mutated gene mutations on brain structure and function is limited. In this study, white matter motor pathway integrity was investigated in ataxia telangiectasia patients using diffusion MRI and probabilistic tractography.

Methods: Diffusion MRI were obtained from 12 patients (age range: 7-22 years, mean: 12 years) and 12 typically developing age matched participants (age range 8-23 years, mean: 13 years). White matter fibre tracking and whole tract statistical analyses were used to assess quantitative fractional anisotropy and mean diffusivity differences along the cortico-ponto-cerebellar, cerebellar-thalamo-cortical, somatosensory and lateral corticospinal tract length in patients using a linear mixed effects model. White matter tract streamline number and apparent fiber density in patient and control tracts were also assessed.

Results: Reduced fractional anisotropy along all analysed patient tracts were observed (p <0.001). Mean diffusivity was significantly elevated in anterior tract locations but was reduced within cerebellar peduncle regions of all patient tracts (p <0.001). Reduced tract streamline number and tract volume in left and right corticospinal and somatosensory tracts were observed in patients (p <0.006). In addition, reduced apparent fibre density in left and right corticospinal and right somatosensory tracts ($p < 0.006$) occurred in patients.

Conclusions: Whole tract analysis of corticomotor, corticospinal and somatosensory pathways in ataxia telangiectasia showed significant white matter degeneration along the

entire length of motor circuits, highlighting that ataxia-telangiectasia gene mutation impacts the cerebellum and multiple other motor circuits in young patients.

1. Introduction

The autosomal recessive neurodegenerative disorder ataxia-telangiectasia (A-T) occurs in approximately 3 per million live births (Woods et al., 1990). ATM (ataxia-telangiectasia mutated) gene mutations give rise to this multisystem disorder (Gatti et al., 1988; Savitsky et al., 1995) which is characterized by progressive cerebellar ataxia, immunodeficiency, sinopulmonary infections, oculocutaneous telangiectasia (Boder and Sedgwick, 1958; Dunn et al., 1964) and elevated serum alpha-fetoprotein levels (Waldmann and McIntire, 1972). The protein kinase ATM, a key player in the cellular response to DNA damage is activated by DNA double-stranded breaks (Lavin, 2008; Shiloh and Ziv, 2013). The ATM protein is also involved in the response to oxidative damage, being activated by oxidative stress (Guo et al., 2010) and may have a more general role in cell homeostasis. Activated ATM phosphorylates a multitude of proteins controlling various cellular processes, specifically cell cycle checkpoint pathways (Beamish et al., 1996) and DNA repair (Shiloh and Ziv, 2013). ATM gene mutations are linked to increased radiosensitivity both in A-T patients (Gotoff et al., 1967; Morgan et al., 1968) and in patient cells in culture (Chen et al., 1978; Taylor et al., 1975). The cause of death in most A-T patients is lymphoreticular malignancy or recurrent chronic respiratory infections (Boder and Sedgwick, 1958; Dunn et al., 1964).

To date, conventional T1- and T2-weighted MRI imaging studies have highlighted hallmark neuropathological features, namely progressive cerebellar atrophy, in A-T (reviewed in

(Sahama et al., 2014b)). From a radiological perspective this has been useful, however such studies provide limited insight into neurodegeneration and its association with loss of connectivity in multiple neural networks. Recently, we reported volume reductions in cortical motor regions in children with A-T using voxel-based morphometry (VBM) applied to structural MRI data (Sahama et al., 2014a). Furthermore we observed WM structural changes within the cerebellum, cerebellar peduncles and in motor regions traversing the posterior limb of the internal capsule using diffusion MRI (dMRI) and tract based spatial statistics (TBSS) (Sahama et al., 2014a). In this approach, diffusion tensor imaging (DTI) was used to measure the preferred direction of water diffusion along WM fiber tracts (Basser et al., 1994). DTI provides quantitative measures of diffusion anisotropy, such as fractional anisotropy (FA), which is thought to reflect axonal WM fiber degeneration (Beaulieu, 2002; Ciccarelli et al., 2006; Johansen-Berg and Rushworth, 2009). Mean diffusivity (MD), a quantitative measure of the mean motion of water considered in all directions, can be used to interrogate pathological cerebral tissue changes, such as demyelination (Alexander et al., 2007). Typically, decreases in FA, and increases in MD reflect WM fiber degeneration (reviewed in (Beaulieu, 2002)).

Although voxel-wise analyses of FA and MD in A-T patients identify altered WM integrity (Sahama et al., 2014a), a limitation of this approach is that it does not provide information about specific WM pathways affected by neurodegenerative changes. When DTI is used in conjunction with probabilistic tractography algorithms, probabilistic maps of specific fiber tracts can be generated, enabling the connectivity of pathways linking multiple brain regions to be interrogated (Ciccarelli et al., 2006; Johansen-Berg and Rushworth, 2009).

DTI and fiber tracking have been applied to study cerebellar - corticomotor networks in a number of ataxic conditions (Habas and Cabanis, 2007; Kitamura et al., 2008; Pagani et al., 2010; Prodi et al., 2013; Rizzo et al., 2011; Solodkin et al., 2011; Ying et al., 2009; Yoon et al., 2006) other than A-T. Although histopathological evidence for collective atrophy in pontocerebellar pathways (Verhagen et al., 2012), altered evoked potentials and myelinated fiber loss in spinal cord sensory pathways (Aguilar et al., 1968; Boder and Sedgwick, 1958; De Leon et al., 1976; Dunn, 1973; Scarpini et al., 1996; Sourander et al., 1966; Stritch, 1966), and demyelination of corticospinal tracts (CST) have been reported in A-T (Agamanolis and Greenstein, 1979; Verhagen et al., 2012), these findings relate to post mortem studies, usually at the end stages of disease. dMRI studies that employ probabilistic tractography to analyze WM pathway integrity and connectivity to multiple brain regions is urgently required to fully understand the impact of the ATM gene mutation on A-T motor circuits.

To this end, the present study employed the use of an "along tract" statistical approach (Colby et al., 2012), whereby diffusion imaging metrics (FA and MD) were measured along the length of lateral CST, somatosensory, cortico-ponto-cerebellar (CPC) and cerebellar-thalamo-cortical (CTC) tracts in young A-T and typically developing age matched participants. Compared to standard "tract-averaged" tractography, which provides one averaged FA and MD value per tract (reviewed in (Colby et al., 2012)), the along tract protocol calculates FA and MD values at consistent intervals along the entire tract length, thereby providing a comprehensive view of the anatomical variation in WM integrity along neural pathways.

In addition to whole tract analysis, A-T WM tract streamline count, tract volume and apparent fiber density (AFD) were analyzed in this study. Tract streamline counts can be used

to detect general degeneration of A-T tracts. Tract volume measures the total voxel volume of all voxels belonging to the tract pathway of interest and when normalized to the intracranial volume (ICV), can provide an informed insight into hemisphere-specific WM changes (Kamson et al., 2015). Similarly, AFD, a tract specific measure derived from the fiber orientation distribution (FOD), allows identification of structural differences along single fiber bundles and assessment of connectivity between two anatomical regions that encompass a specific tract (Raffelt et al., 2012). Using whole tract analysis, WM tract streamline count, tract volume and AFD measures, we present novel findings depicting loss in WM integrity along the entire tract length of CPC, CTC, somatosensory and CST pathways in A-T.

2. Methods

2.1 Participants

MRI data were acquired from 12 patients with A-T (age mean SD: 12± 5.34; age range: 7-22 years, 6 Male) and 12 healthy, age matched typically developing participants (age mean SD: 12.67± 5.28; age range 8-23 years, 4 Male). All patients have been clinically diagnosed with A-T, according to the recent World Health Organization recommendations (Notarangelo et al., 2004) including genetic testing. Informed consent was given by all subjects and parents in accordance with our Human Ethics Institutional Review Board and the Declaration of Helsinki.

2.2 Clinical scoring

The A-T Neuro Examination Scale Toolkit (A-T NEST), which was refined from a quantitative 10-point scale (Crawford et al., 2000), was used to clinically observe A-T patients. This scaling system is a sensitive tool that specifically accounts for the multi-

dimensional complexity and heterogeneity of A-T neurological deficits (personal communication with Dr. Thomas Crawford, Professor of Neurology and Pediatrics at the John Hopkins Hospital).

2.3 Image acquisition

MRI data were acquired using a 3T MRI scanner (Siemens Trio, Erlangen, Germany) with TQ gradients (45 mT/m, slew rate 200 T/m/s), using a 12 element Tim head array. A 0.9 mm isotropic 3D T1 Magnetization Prepared Rapid Gradient Echo (MPRAGE) sequence was used to acquire a high resolution structural image. The imaging parameters were: field of view 23×23×17.3 cm; TR/TE/TI 1900/2.32/900 ms; flip angle 9°; matrix size 192×512×512×1 cm. Diffusion MRI acquisition consisted of a High Angular Resolution Diffusion Imaging (HARDI) sequence with the following parameters: 60 axial slices; 2.5 mm slice thickness; field of view 30×30 cm; TR/TE 9500/116 ms; acquisition matrix 128×128, resulting in an in-plane resolution of 2.34×2.34 mm. To reduce susceptibility distortions, parallel imaging with an acceleration factor of 2 was employed. Sixty-four diffusion weighted images were acquired at b = 3000 s mm^{-2}, along with one minimally diffusion weighted image (b = 0). The acquisition time for the diffusion dataset was 9:40 minutes. Two 2-dimensional gradient-recalled echo images (36 axial slices; 3 mm slice thickness with 0.75 mm gap; field of view 19.2×19.2 cm; TR/TE1/TE2 488/4.92/7.38 ms; acquisition matrix 64×64) were used to acquire a field map for diffusion data, to assist distortion correction due to susceptibility inhomogeneity.

2.4 Diffusion processing

Diffusion weighted images were corrected for subject motion by identifying head movement within volumes using the discontinuity index and subsequently using the Fit Model to All

Measurements (FMAM) method to correct movement between volumes (Bai and Alexander, 2008). Susceptibility distortions were corrected using the field map employing FMRIB's Utility for Geometrically Unwarping EPIs (FUGUE) (Jenkinson, 2003) and Phase Region Expanding Labeler for Unwrapping Discrete Estimates (PRELUDE) (Jenkinson et al., 2004) in raw image space (both contained within FMRIB's Software Library (FSL)) (Jenkinson et al., 2012), with signal intensity correction (Jones, 2010). Motion artefacts were identified and replaced using Detection and Replacement of Outliers Prior to Resampling (DROP-R) (Morris et al., 2011), modified from the originally proposed method to incorporate an outlier detection technique suitable for high b-value diffusion data (Pannek et al., 2012). Using the corrected data, the fiber orientation distribution (FOD) was estimated using the constrained spherical deconvolution (CSD) method within the MRtrix package (https://github.com/jdtournier/mrtrix3) (Tournier et al., 2007). MRtrix was also used to generate FA and MD maps.

2.5 Tractography

Probabilistic tractography was performed using MRtrix3. To extract WM fiber tracks of interest, anatomically constrained tractography (ACT) (Smith et al., 2012) was performed. T1 co-registration to the diffusion imaging series, and subsequent FSL BET/FAST/FIRST processing on structural data as per the MRtrix 3 'act_anat_prepare_fsl' script was conducted to produce a five tissue types mask, to generate whole brain tractograms comprising fifty-million streamlines (Tournier et al., 2012). Wholebrain tractograms were subsequently processed using the Spherical-deconvolution Informed Filtering of Tractograms (SIFT) procedure introduced in MRtrix3, resulting in twenty-five million streamlines (Smith et al., 2013), to reduce false positive streamlines. The MRtrix package was used to select regions-of-interest (ROIs) to enable extraction of the CPC, CTC, CST and somatosensory fiber tracks

from SIFTed wholebrain tractograms. ROIs, particularly for CST and somatosensory tracts, were identified using established target regions specific to children (Kamali et al., 2010; Kumar et al., 2009) and verified manually by an expert child neurologist (SF). ROIs were placed in the precentral and postcentral gyrus and spinal cord for CST, postcentral gyrus and spinal cord for somatosensory tracts and cerebral hemispheres and opposing medial cerebellar peduncle and superior cerebellar peduncle regions for CPC and CTC tracts respectively (Fig. 1).

2.6 Along Tract Statistical analysis

Quantitative tractography metrics (FA and MD) were derived using whole tract methodology. Motor circuits were defined according to 'start' and 'end' ROIs (visualized in Fig. 1 first and second rows respectively) and cropped at 'end' ROIs to ensure similar tract length of all tracts within the circuit. Further removal of spurious tracts was achieved by rejecting 10% of the longest tracts in motor circuits. FA and MD were sampled by automated segmentation of individual tracts into 20 locations (bins) of equal streamline point count to ensure minimal data variance in metrics along the tract. This approach ensures anatomically coincident bins to be sampled along each tract of interest for each participant. FA and MD values within one patient were statistically compared to a corresponding age matched control at each bin along each tract, using a linear mixed effects model. Bin location along the tract was associated to an anatomical landmark in individual patients to pinpoint WM changes by brain region in A-T. P-values less than or equal to 0.001 were considered statistically significant after p-value alpha adjustment for 40 multiple tests of hypotheses based on bin number (20) and condition (control or patient (2)) per bin, equating to the evaluation of individual bins in each subject group. In addition, MD values in all control and patient ROIs at the level of the cerebral motor cortex (parietal cortex) and the cerebellar peduncles were computed using the 'fslstats'

command, part of FSL (Jenkinson et al., 2012) to cross-check MD values in selected corticomotor pathways. P-values less than or equal to 0.005 were considered statistically significant for this analysis after p-value alpha adjustment for 11 multiple tests of hypotheses, corresponding to the total number of ROIs selected. All statistical analyses and data visualization were performed using the R statistical environment (Team, 2014).

2.7 WM Tract Streamline Number, Tract Volume and AFD Statistical analysis

As tensor based diffusivity measures are voxel-average quantities and not tract specific in voxels containing complex fiber architecture, streamline number, tract volume and AFD metrics were also investigated in this study. Streamline number, tract volume and AFD in A-T and control participants were calculated and averaged based on patient or control condition per tract due to the small number of subjects undergoing analysis. Tract volume was derived using the 'fslstats' command, part of FSL (Jenkinson et al., 2012) and normalized based on ICV (Kamson et al., 2015). At high diffusion gradient b-values, the AFD is proportional to the intra-axonal volume of axons associated with that FOD lobe (Raffelt et al., 2012). Summing the AFD integral for all FOD lobes associated with the tract streamlines enables generation of a measure related to the total intra-axonal tract volume. The AFD integral is normalized by dividing by the mean streamline length to yield a measure proportional to tract cross sectional area, and can be used to compare tract specific degeneration in A-T participants and age-matched control participants. AFD values (corrected and uncorrected for partial volume effects) were calculated using the 'afdconnectivity' command in MRtrix3 (https://github.com/jdtournier/mrtrix3). Parametric test assumptions of homogeneity of variance and normal distribution were assessed and confirmed prior to all statistical analyses. Statistical differences in streamline number, tract volume and AFD between patient and control conditions were computed using an independent t-test and visualized using the R

statistical environment (Team, 2014). Streamline number, tract volume and AFD measures were considered significant after p-value alpha adjustment for 8 multiple tests of hypotheses based on number of tracts analysed ($p < 0.006$).

3. Results

3.1 Clinical observations

Heterogenous ataxia and movement disorder was observed in A-T patients, irrespective of age. Clinical scores in four young patients depicted advanced WM degeneration, with variations in ataxic mobility (walking and standing) and neuropathy, the absence of ankle, knee and bicep tendon reflexes and loss of proprioception in the extremities (Patients 2, 7, 9 and 11, 7-10 years of age, Inline supplementary material, Table 1).

3.2 Whole Tract Analysis of Control and Patient WM Tracts

Lateral CST, CPC, CTC and somatosensory tracts descend from the cerebral motor cortex at the level of the parietal lobe to the cerebellar peduncles collectively, connecting these two regions. Compared to motor pathways in age matched controls, A-T CST and somatosensory pathways display a morphological thinning of tracts at the level of the thalamus in the coronal view. In addition, A-T CPC and CTC pathways display morphological thinning of tracts in the cerebellum at the position of the medial cerebellar peduncles (Fig. 2).

Significant FA reductions along the lateral CST, CPC, CTC and somatosensory tracts were observed collectively in A-T patients compared to controls ($p < 0.001$, Fig. 3, for all tracts). Areas of non-significant FA changes in the left CTC at 5%, 11% and 32% of the tract length and in the right CTC at 0% and 5% of the tract length were observed in A-T (Fig. 3, denoted

by 'N'). A general decrease in average FA magnitude (approximated to two decimal places and averaged across age) between control and patient groups were observed along all analysed corticomotor tracts (Inline supplementary material Table 2).

A significant increase in MD in all A-T WM pathways was recorded at the level of the cerebral cortex (0%-50% of tract length), however, a paradoxical decrease in MD was observed at the level of the cerebellar peduncles (50%-100% of tract length) in all tracts ($p <$ 0.001, Fig. 4). To cross-check the decrease in MD, a cross-examination of ROIs at the cerebral (precentral and postcentral gyrus) and cerebellar peduncle level in patients and controls was conducted and revealed neither an increase nor decrease in MD at the cerebral and cerebellar levels in these ROIs respectively, in patients (data not shown). In addition, static change in average MD magnitude (approximated to two decimal places and averaged across age) between control and patient groups was observed along all analysed corticomotor tracts (Inline supplementary material Table 2). Areas of non-significant MD change in the right CPC tract at 32% of the tract length and in the right CTC tract at 0% and 37% of the tract length were observed in patients (Fig. 4, denoted by 'N').

3.3 Streamline Number and Tract Volume Analysis

Reduced streamline number in left and right CST and right somatosensory tracts was observed in A-T patients (p<0.006, Fig. 5A). Tract volume reductions were observed in the left CTC, left somatosensory, right CPC and right CST A-T tracts (p<0.006, Fig. 5C).

3.4 AFD Analysis

Reductions in fiber integrity in right CST and somatosensory tracts in A-T subjects were observed compared to controls (p<0.006, Fig. 5B). Reductions in fiber integrity in left and right CST and right somatosensory tracts in A-T subjects were also observed when corrected for partial volume effects (p<0.006, Fig. 5D). Although not reaching a level of significance, the left CST (Fig. 5B), left somatosensory and right CPC tracts (Fig. 5B and D) displayed a trend towards reduced integrity in A-T subjects. Higher AFD was found in the right CTC tracts in A-T (p<0.006, Fig. 5B), however this result was not significant in partial volume corrected data (Fig. 5D), suggesting the influence of small streamline numbers delineating in this pathway.

4. Discussion

dMRI and probabilistic tractography has not yet been applied to A-T despite its use in investigating cerebellar WM degeneration in multi-spectrum ataxic disorders (Habas and Cabanis, 2007; Pagani et al., 2010; Prodi et al., 2013). In this study, WM microstructural analysis of cerebellar-corticomotor and corticospinal pathways was conducted in a sizeable A-T cohort using an appropriate analysis pipeline. Specifically, anatomical variation in WM integrity along motor tract length was demonstrated for the first time in A-T.

Neurodegeneration of lateral CST, CPC, CTC and somatosensory tracts along tract length were collectively observed among all A-T patients in this study. Analysis of FA and MD differences along the whole tract resulted in p-values with a magnitude of less than or equal to 10^{-6} (data not shown), indicating significant neurodegenerative change among A-T corticomotor and corticospinal tracts compared to age matched control participants. FA reductions in cerebral cortex, cerebellar and spinal cord regions suggest involvement of these areas in young A-T patients, and provide an insight into the advanced state of neuropathy,

White Matter Tracts in Ataxia Telangiectasia   Sahama et al

absence of reflexes (ankle, knee and bicep tendons) and proprioception observed in the extremities of these patients. While cerebellar degeneration is a well-established finding in A-T, structural changes in the cerebral motor cortex and spinal cord, particularly in histopathological studies, has been confined mainly to older A-T patients (reviewed (Sahama et al., 2014b)) and sparingly in young patients (Chung et al., 1994; De Leon et al., 1976). Cerebral abnormalities in structural MRI studies have also been observed largely in adult A-T patients (Hoche et al., 2014; Lin et al., 2013; Sardanelli et al., 1995), however exceptional cases in early A-T have been noted (Chung et al., 1994). Our current findings of cerebellar, somatosensory and spinal cord neurodegeneration, and our previous observations of reduced grey matter density in A-T motor regions (Sahama et al., 2014a), provide evidence that the thalamus, precentral gyrus and postcentral gyrus are likely affected in our young A-T patient cohort. To our knowledge, involvement of these cortical areas has not previously been reported in imaging studies in A-T, however reduced metabolism in the fusiform gyrus of the cerebral cortex has been observed using ^{18}F-FDG PET imaging (Volkow et al., 2014).

In contrast to MD findings in neurodegenerative conditions (reviewed in (Beaulieu, 2002)), a marked decrease in MD at the cerebellar peduncles was observed for all A-T tracts in this study, despite the lack of MD differences at cerebral and cerebellar ROIs in patients and controls (data not shown) and the static change in average MD magnitude across patient age in corticomotor pathways. MD reductions have previously been reported during the hyperacute stages of ischemic stroke. In stroke, MD reduction has been postulated to be caused by cell swelling, where post ischemic energy failure causes sodium (Na+), potassium (K+)-ATPase transmembrane pump failure, inducing loss of ion homeostasis, excitatory amino acid release and water influx from extracellular to intracellular cell space (reviewed in (Jones, 2011)). Such marked changes in ion homeostasis is unlikely to occur in A-T, since

A-T neurons differentiated from induced pluripotent stem cells display similar voltage-gated potassium and sodium currents and action potential discharge as healthy neurons. Nevertheless, defective neuronal growth associated protein and potassium channel-interacting protein expression was observed in that study (Carlessi et al., 2014). In a recent study, neural progenitors differentiated from olfactory neurosphere-derived cells in A-T patients were defective in neurite formation, neurite number and length (Stewart et al., 2013). In addition, a mouse model of A-T displayed decreases in the duration of calcium and sodium firing in Purkinje cells, with the presence of progressive calcium deficit despite normal resting membrane potential, input resistance or anomalous rectification (potassium currents) in cells. Calcium deficits were caused by decreases in calcium currents and were related to cell death in other tested mutant mice (Chiesa et al., 2000). While these findings do not provide evidence for an imbalance in ion homeostasis in A-T neurons, they nevertheless indicate A-T neuronal cell abnormalities which could fit with MD reduction in the A-T cerebellum and spinal cord in the current study. MD reductions in A-T may also be markers of neurodegeneration, as restricted and hindered diffusion have been reported to decrease the apparent diffusivity of water (Le Bihan, 1995; Tuor et al., 2014), particularly where acute Wallerian degeneration is involved (Musson and Romanowski, 2010). Currently, it is unclear whether neurodegeneration in A-T involves Wallerian degeneration in associated corticomotor pathways. Future use of longitudinal studies to track neurodegeneration in patients from early age to chronic disease states may allow the clarification of such degenerative involvement. Nevertheless, cell death in cerebellar regions is prevalent in A-T and are correlated with MD reductions, as are astrocyte reactivity and microglial/macrophage activation within the cerebral cortex (Tuor et al., 2014). Therefore MD reductions in this study may also reflect chronic oxidative stress-induced Purkinje cell death, thought to be the primary cause of neurodegeneration, as a consequence of failure to actively regulate

oxidative stress levels in the A-T cerebellum (reviewed in (Sahama et al., 2014b)). Overall, the unpredictable combination of demyelination, axon loss, gliosis, and inflammation in individual A-T patients may result in competing influences of quantitative DTI metrics in brain regions. To improve DTI metric specificity in A-T, a combination of multiple imaging measures (e.g., T1, T2, magnetization transfer, perfusion, fast/slow diffusion, etc.) (Alexander et al., 2007) is required.

Reductions in WM tract streamline number, tract volume and AFD measures coincided with FA reduction in robust WM tracts, in particular, in the left and right CST and somatosensory tracts in A-T. AFD connectivity and streamline number are highly related to one another when ACT and SIFT protocols are used, however, the localization of neurodegenerative changes to the right hemisphere in A-T is unprecedented. Previously, we reported significant cerebellar-corticomotor pathway changes localized to only the left cerebral hemisphere in A-T using a different analysis technique, namely TBSS (Smith et al., 2006; Smith et al., 2004), with no clear correlation to clinical observations (Sahama et al., 2014a). TBSS is a voxelwise analysis technique that is less specific to probing the integrity of individual WM pathways. Although we reported only significant changes in FA and MD within left hemispheric WM pathways, we did observe similar changes within corresponding right hemisphere WM (uncorrected) that did not reach a level of statistical significance. The observation of both left and right hemisphere WM motor tract involvement in the current analysis may indicate the added sensitivity of the more specific along tract analysis approach. In structural imaging, there is little evidence of right cerebral laterality in A-T, particularly in the present A-T cohort (data not shown), however, post-mortem studies have recorded lesions exclusive to the right thalamus (De Leon et al., 1976) and right temporal white matter (Monaco et al., 1988). Localized WM maturation in the control population may also contribute to the laterality

observed in streamline number and AFD metrics in our A-T patients. Indeed, voxel-wise analysis and DTI imaging in healthy children and adults have revealed increased FA and decreased MD with increasing age in the right temporal lobe (Qiu et al., 2008) and right inferior longitudinal fasciculus (Schmithorst et al., 2002). These observations however, are cohort specific, thus WM tract streamline number and AFD laterality in this study may also be specific to our patient cohort.

Low streamline numbers in control and A-T CPC and CTC tracts highlight the challenge of robustly defining these pathways using dMRI acquisition schemes suitable for clinical populations (less than 10 minute scan time). Given this limitation, some caution needs to be observed when deferring information about degeneration processes occurring within these pathways. It should be noted that only streamlines hitting both cerebellar and cortical targets were included in this study. Many streamlines projecting from the cerebellum failed to project into the motor cortex and therefore has the potential for biasing streamline number analyses. Clearly, larger cohorts are needed to better define integrity of these motor pathways.

The primary limitation of this study is the small A-T cohort that underwent analysis and impacted on the findings. Fewer than 50 A-T cases have been reported in Australia overall (Miles, 2011), with this study's clinical population recruited from the only research clinic nationally, specializing in health care for an estimated 54% of the national A-T population. In addition, the use of non-sedated MRI scanning in this study has restricted the age range of patients to age 6 and above. To understand the extent of multiple affected brain areas and their sequence of development in early and advanced A-T, larger collaborative studies across multiple research sites (Anscombe, 2013) is required. Another significant limitation is the

inability of dMRI to accurately resolve crossing fiber tracts in complex WM architecture (Jones, 2008). Specifically, multiple fibres that cross within each voxel provide unintuitive quantitative DTI measures. Indeed, in neurodegenerative conditions, increased anisotropy can be observed in regions of crossing fibers (Douaud et al., 2011), and is observed in average FA magnitude values per bin in the present study. In cases of Wallerian degeneration, almost no change in diffusion anisotropy can be detected where degenerated pathways cross other tracts (Pierpaoli et al., 2001). The use of a higher order model can resolve multiple crossing fibres within each voxel (Tournier et al., 2007) and can improve the accuracy of tract delineations with tractography however, paradoxical changes in FA and MD (calculated using the diffusion tensor model), as seen in the measure of A-T WM integrity in the present study, can confound interpretation of results. Multiple imaging metrics in combination with higher order models allow complex neurodegenerative processes in A-T to be interpreted comprehensively thus streamline number, tract volume and AFD measures were introduced in this study to obtain a broader understanding of the neurological processes that contribute to A-T neurodegeneration.

In future, investigation of cerebro-olivocerebellar and cerebro-reticular cerebellar pathways is required in A-T due to involvement of the inferior olives (Agamanolis and Greenstein, 1979; Amromin et al., 1979; De Leon et al., 1976; Stritch, 1966; Verhagen et al., 2012) and the medullary reticular formation (De Leon et al., 1976) in the disease. The dorsal spinocerebellar tracts in A-T (De Leon et al., 1976; Solitare and Lopez, 1967) also warrant further investigation but were excluded in the current study due to insufficient tract length in brain MRI for whole tract analysis. In future, spinal cord MRI could be employed to effectively capture these tracts in their entirety for analysis.

Acknowledgments

References

Agamanolis, D.P., Greenstein, J.I., 1979. Ataxia-telangiectasia. Report of a case with Lewy bodies and vascular abnormalities within cerebral tissue. J Neuropathol Exp Neurol 38, 475-489.

Aguilar, M.J., Kamoshita, S., Landing, B.H., Boder, E., Sedgwick, R.P., 1968. Pathological observations in ataxia-telangiectasia. A report of five cases. J Neuropathol Exp Neurol 27, 659-676.

Alexander, A.L., Lee, J.E., Lazar, M., Field, A.S., 2007. Diffusion tensor imaging of the brain. Neurotherapeutics 4, 316-329.

Amromin, G.D., Boder, E., Teplitz, R., 1979. Ataxia-telangiectasia with a 32 year survival. A clinicopathological report. J Neuropathol Exp Neurol 38, 621-643.

Anscombe, C., 2013. New technology could shed light on treatment of rare genetic condition. Health News.

Bai, Y., Alexander, P., 2008. Model-based registration to correct for motion between acquisitions in diffusion MR imaging. IEEE International Symposium on Biomedical Imaging: From Nano to Macro.

Basser, P.J., Mattiello, J., LeBihan, D., 1994. Estimation of the effective self-diffusion tensor from the NMR spin echo. J Magn Reson B 103, 247-254.

Beamish, H., Williams, R., Chen, P., Lavin, M.F., 1996. Defect in multiple cell cycle checkpoints in ataxia-telangiectasia postirradiation. J Biol Chem 271, 20486-20493.

Beaulieu, C., 2002. The basis of anisotropic water diffusion in the nervous system - a technical review. NMR Biomed 15, 435-455.

Boder, E., Sedgwick, R.P., 1958. Ataxia-telangiectasia; a familial syndrome of progressive cerebellar ataxia, oculocutaneous telangiectasia and frequent pulmonary infection. Pediatrics 21, 526-554.

Carlessi, L., Fusar Poli, E., Bechi, G., Mantegazza, M., Pascucci, B., Narciso, L., Dogliotti, E., Sala, C., Verpelli, C., Lecis, D., Delia, D., 2014. Functional and molecular defects of hiPSC-derived neurons from patients with ATM deficiency. Cell Death Dis 5, e1342.

Chen, P.C., Lavin, M.F., Kidson, C., Moss, D., 1978. Identification of ataxia telangiectasia heterozygotes, a cancer prone population. Nature 274, 484-486.

Chiesa, N., Barlow, C., Wynshaw-Boris, A., Strata, P., Tempia, F., 2000. Atm-deficient mice Purkinje cells show age-dependent defects in calcium spike bursts and calcium currents. Neuroscience 96, 575-583.

Chung, E.O., Bodensteiner, J.B., Noorani, P.A., Schochet, S.S., 1994. Cerebral White-Matter Changes Suggesting Leukodystrophy in Ataxia Telangiectasia. Journal of Child Neurology 9, 31-35.

Ciccarelli, O., Behrens, T.E., Altmann, D.R., Orrell, R.W., Howard, R.S., Johansen-Berg, H., Miller, D.H., Matthews, P.M., Thompson, A.J., 2006. Probabilistic diffusion tractography: a potential tool to assess the rate of disease progression in amyotrophic lateral sclerosis. Brain 129, 1859-1871.

Colby, J.B., Soderberg, L., Lebel, C., Dinov, I.D., Thompson, P.M., Sowell, E.R., 2012. Along-tract statistics allow for enhanced tractography analysis. Neuroimage 59, 3227-3242.

Crawford, T.O., Mandir, A.S., Lefton-Greif, M.A., Goodman, S.N., Goodman, B.K., Sengul, H., Lederman, H.M., 2000. Quantitative neurologic assessment of ataxia-telangiectasia. Neurology 54, 1505-1509.

De Leon, G.A., Grover, W.D., Huff, D.S., 1976. Neuropathologic changes in ataxia-telangiectasia. Neurology 26, 947-951.

Douaud, G., Jbabdi, S., Behrens, T.E., Menke, R.A., Gass, A., Monsch, A.U., Rao, A., Whitcher, B., Kindlmann, G., Matthews, P.M., Smith, S., 2011. DTI measures in crossing-fibre areas: increased diffusion anisotropy reveals early white matter alteration in MCI and mild Alzheimer's disease. Neuroimage 55, 880-890.

Dunn, H.G., 1973. Nerve conduction studies in children with Friedreich's ataxia and ataxia-telangiectasia. Dev Med Child Neurol 15, 324-337.

Dunn, H.G., Meuwissen, H., Livingstone, C.S., Pump, K.K., 1964. ATAXIA-TELANGIECTASIA. Can Med Assoc J 91, 1106-1118.

Gatti, R.A., Berkel, I., Boder, E., Braedt, G., Charmley, P., Concannon, P., Ersoy, F., Foroud, T., Jaspers, N.G., Lange, K., et al., 1988. Localization of an ataxia-telangiectasia gene to chromosome 11q22-23. Nature 336, 577-580.

Gotoff, S.P., Amirmokri, E., Liebner, E.J., 1967. Ataxia telangiectasia. Neoplasia, untoward response to x-irradiation, and tuberous sclerosis. Am J Dis Child 114, 617-625.

Guo, Z., Kozlov, S., Lavin, M.F., Person, M.D., Paull, T.T., 2010. ATM activation by oxidative stress. Science 330, 517-521.

Habas, C., Cabanis, E.A., 2007. Anatomical parcellation of the brainstem and cerebellar white matter: a preliminary probabilistic tractography study at 3 T. Neuroradiology 49, 849-863.

Hoche, F., Frankenberg, E., Rambow, J., Theis, M., Harding, J.A., Qirshi, M., Seidel, K., Barbosa-Sicard, E., Porto, L., Schmahmann, J.D., Kieslich, M., 2014. Cognitive phenotype in ataxia-telangiectasia. Pediatr Neurol 51, 297-310.

Jenkinson, M., 2003. Fast, automated, N-dimensional phase-unwrapping algorithm. Magn Reson Med 49, 193-197.

Jenkinson, M., Beckmann, C.F., Behrens, T.E., Woolrich, M.W., Smith, S.M., 2012. FSL. Neuroimage 62, 782-790.

Jenkinson, M., Wilson, J.L., Jezzard, P., 2004. Perturbation method for magnetic field calculations of nonconductive objects. Magn Reson Med 52, 471-477.

Johansen-Berg, H., Rushworth, M.F., 2009. Using diffusion imaging to study human connectional anatomy. Annu Rev Neurosci 32, 75-94.

Jones, D.K., 2008. Studying connections in the living human brain with diffusion MRI. Cortex 44, 936-952.

Jones, D.K., 2010. Precision and accuracy in diffusion tensor magnetic resonance imaging. Top Magn Reson Imaging 21, 87-99.

Jones, D.K., 2011. Diffusion MRI: Theory, Methods and Applications. Oxford University Press, New York.

Kamali, A., Kramer, L.A., Frye, R.E., Butler, I.J., Hasan, K.M., 2010. Diffusion tensor tractography of the human brain cortico-ponto-cerebellar pathways: a quantitative preliminary study. J Magn Reson Imaging 32, 809-817.

Kamson, D.O., Juhasz, C., Chugani, H.T., Jeong, J.W., 2015. Novel diffusion tensor imaging technique reveals developmental streamline volume changes in the corticospinal tract associated with leg motor control. Brain Dev 37, 370-375.

Kitamura, K., Nakayama, K., Kosaka, S., Yamada, E., Shimada, H., Miki, T., Inoue, Y., 2008. Diffusion tensor imaging of the cortico-ponto-cerebellar pathway in patients with adult-onset ataxic neurodegenerative disease. Neuroradiology 50, 285-292.

Kumar, A., Juhasz, C., Asano, E., Sundaram, S.K., Makki, M.I., Chugani, D.C., Chugani, H.T., 2009. Diffusion tensor imaging study of the cortical origin and course of the corticospinal tract in healthy children. AJNR Am J Neuroradiol 30, 1963-1970.

Lavin, M.F., 2008. Ataxia-telangiectasia: from a rare disorder to a paradigm for cell signalling and cancer. Nat Rev Mol Cell Biol 9, 759-769.

Le Bihan, D., 1995. Molecular diffusion, tissue microdynamics and microstructure. NMR Biomed 8, 375-386.

Lin, D.D., Barker, P.B., Lederman, H.M., Crawford, T.O., 2013. Cerebral Abnormalities in Adults with Ataxia-Telangiectasia. AJNR Am J Neuroradiol.

Miles, J., 2011. A charity that begins at home. The Courier-Mail.

Monaco, S., Nardelli, E., Moretto, G., Cavallaro, T., Rizzuto, N., 1988. Cytoskeletal pathology in ataxia-telangiectasia. Clin Neuropathol 7, 44-46.

Morgan, J.L., Holcomb, T.M., Morrissey, R.W., 1968. Radiation reaction in ataxia telangiectasia. Am J Dis Child 116, 557-558.

Morris, D., Nossin-Manor, R., Taylor, M.J., Sled, J.G., 2011. Preterm neonatal diffusion processing using detection and replacement of outliers prior to resampling. Magn Reson Med 66, 92-101.

Musson, R., Romanowski, C., 2010. Restricted diffusion in Wallerian degeneration of the middle cerebellar peduncles following pontine infarction. Pol J Radiol 75, 38-43.

Notarangelo, L., Casanova, J.L., Fischer, A., Puck, J., Rosen, F., Seger, R., Geha, R., International Union of Immunological Societies Primary Immunodeficiency diseases classification, c., 2004. Primary immunodeficiency diseases: an update. J Allergy Clin Immunol 114, 677-687.

Pagani, E., Ginestroni, A., Della Nave, R., Agosta, F., Salvi, F., De Michele, G., Piacentini, S., Filippi, M., Mascalchi, M., 2010. Assessment of brain white matter fiber bundle atrophy in patients with Friedreich ataxia. Radiology 255, 882-889.

Pannek, K., Raffelt, D., Bell, C., Mathias, J.L., Rose, S.E., 2012. HOMOR: higher order model outlier rejection for high b-value MR diffusion data. Neuroimage 63, 835-842.

Pierpaoli, C., Barnett, A., Pajevic, S., Chen, R., Penix, L.R., Virta, A., Basser, P., 2001. Water diffusion changes in Wallerian degeneration and their dependence on white matter architecture. Neuroimage 13, 1174-1185.

Prodi, E., Grisoli, M., Panzeri, M., Minati, L., Fattori, F., Erbetta, A., Uziel, G., D'Arrigo, S., Tessa, A., Ciano, C., Santorelli, F.M., Savoiardo, M., Mariotti, C., 2013. Supratentorial and pontine MRI abnormalities characterize recessive spastic ataxia of Charlevoix-Saguenay. A comprehensive study of an Italian series. Eur J Neurol 20, 138-146.

Qiu, D., Tan, L.H., Zhou, K., Khong, P.L., 2008. Diffusion tensor imaging of normal white matter maturation from late childhood to young adulthood: voxel-wise evaluation of mean diffusivity, fractional anisotropy, radial and axial diffusivities, and correlation with reading development. Neuroimage 41, 223-232.

Raffelt, D., Tournier, J.D., Rose, S., Ridgway, G.R., Henderson, R., Crozier, S., Salvado, O., Connelly, A., 2012. Apparent Fibre Density: a novel measure for the analysis of diffusion-weighted magnetic resonance images. Neuroimage 59, 3976-3994.

Rizzo, G., Tonon, C., Valentino, M.L., Manners, D., Fortuna, F., Gellera, C., Pini, A., Ghezzo, A., Baruzzi, A., Testa, C., Malucelli, E., Barbiroli, B., Carelli, V., Lodi, R., 2011. Brain diffusion-weighted imaging in Friedreich's ataxia. Mov Disord 26, 705-712.

Sahama, I., Sinclair, K., Fiori, S., Pannek, K., Lavin, M., Rose, S., 2014a. Altered corticomotor-cerebellar integrity in young ataxia telangiectasia patients. Mov Disord 29, 1289-1298.

Sahama, I., Sinclair, K., Pannek, K., Lavin, M., Rose, S., 2014b. Radiological imaging in ataxia telangiectasia: a review. Cerebellum 13, 521-530.

Sardanelli, F., Parodi, R.C., Ottonello, C., Renzetti, P., Saitta, S., Lignana, E., Mancardi, G.L., 1995. Cranial MRI in ataxia-telangiectasia. Neuroradiology 37, 77-82.

Savitsky, K., Bar-Shira, A., Gilad, S., Rotman, G., Ziv, Y., Vanagaite, L., Tagle, D.A., Smith, S., Uziel, T., Sfez, S., Ashkenazi, M., Pecker, I., Frydman, M., Harnik, R., Patanjali, S.R., Simmons, A., Clines, G.A., Sartiel, A., Gatti, R.A., Chessa, L., Sanal, O., Lavin, M.F., Jaspers, N.G., Taylor, A.M., Arlett, C.F., Miki, T., Weissman, S.M., Lovett, M., Collins, F.S., Shiloh, Y., 1995. A single ataxia telangiectasia gene with a product similar to PI-3 kinase. Science 268, 1749-1753.

Scarpini, C., Mondelli, M., Guazzi, G.C., Federico, A., 1996. Ataxia-telangiectasia: somatosensory, brainstem auditory and motor evoked potentials in six patients. Dev Med Child Neurol 38, 65-73.

Schmithorst, V.J., Wilke, M., Dardzinski, B.J., Holland, S.K., 2002. Correlation of white matter diffusivity and anisotropy with age during childhood and adolescence: a cross-sectional diffusion-tensor MR imaging study. Radiology 222, 212-218.

Shiloh, Y., Ziv, Y., 2013. The ATM protein kinase: regulating the cellular response to genotoxic stress, and more. Nat Rev Mol Cell Biol 14, 197-210.

Smith, R.E., Tournier, J.D., Calamante, F., Connelly, A., 2012. Anatomically-constrained tractography: improved diffusion MRI streamlines tractography through effective use of anatomical information. Neuroimage 62, 1924-1938.

Smith, R.E., Tournier, J.D., Calamante, F., Connelly, A., 2013. SIFT: Spherical-deconvolution informed filtering of tractograms. Neuroimage 67, 298-312.

Smith, S.M., Jenkinson, M., Johansen-Berg, H., Rueckert, D., Nichols, T.E., Mackay, C.E., Watkins, K.E., Ciccarelli, O., Cader, M.Z., Matthews, P.M., Behrens, T.E., 2006. Tract-based spatial statistics: voxelwise analysis of multi-subject diffusion data. Neuroimage 31, 1487-1505.

Smith, S.M., Jenkinson, M., Woolrich, M.W., Beckmann, C.F., Behrens, T.E., Johansen-Berg, H., Bannister, P.R., De Luca, M., Drobnjak, I., Flitney, D.E., Niazy, R.K., Saunders, J., Vickers, J., Zhang, Y., De Stefano, N., Brady, J.M., Matthews, P.M., 2004. Advances in functional and structural MR image analysis and implementation as FSL. Neuroimage 23 Suppl 1, S208-219.

Solitare, G.B., Lopez, V.F., 1967. Louis-bar's syndrome (ataxia-telangiectasia). Neuropathologic observations. Neurology 17, 23-31.

Solodkin, A., Peri, E., Chen, E.E., Ben-Jacob, E., Gomez, C.M., 2011. Loss of intrinsic organization of cerebellar networks in spinocerebellar ataxia type 1: correlates with disease severity and duration. Cerebellum 10, 218-232.

Sourander, P., Bonnevier, J.O., Olsson, Y., 1966. A case of ataxia-telangiectasia with lesions in the spinal cord. Acta Neurol Scand 42, 354-366.

Stewart, R., Kozlov, S., Matigian, N., Wali, G., Gatei, M., Sutharsan, R., Bellette, B., Wraith-Kijas, A., Cochrane, J., Coulthard, M., Perry, C., Sinclair, K., Mackay-Sim, A., Lavin, M.F., 2013. A patient-derived olfactory stem cell disease model for ataxia-telangiectasia. Hum Mol Genet 22, 2495-2509.

Stritch, S.J., 1966. Pathological findings in three cases of ataxia-telangiectasia. J Neurol Neurosurg Pyschiatr 29, 489–499.

Taylor, A.M., Harnden, D.G., Arlett, C.F., Harcourt, S.A., Lehmann, A.R., Stevens, S., Bridges, B.A., 1975. Ataxia telangiectasia: a human mutation with abnormal radiation sensitivity. Nature 258, 427-429.

Team, R.C., 2014. R: A language and environment for statistical computing. . R Foundation for Statistical Computing, Vienna, Austria.

Tournier, J.D., Calamante, F., Connelly, A., 2007. Robust determination of the fibre orientation distribution in diffusion MRI: non-negativity constrained super-resolved spherical deconvolution. Neuroimage 35, 1459-1472.

Tournier, J.D., Calamante, F., Connelly, A., 2012. MRtrix: Diffusion tractography in crossing fiber regions. International Journal of Imaging Systems and Technology 22, 53-66.

Tuor, U.I., Morgunov, M., Sule, M., Qiao, M., Clark, D., Rushforth, D., Foniok, T., Kirton, A., 2014. Cellular correlates of longitudinal diffusion tensor imaging of axonal degeneration following hypoxic-ischemic cerebral infarction in neonatal rats. Neuroimage Clin 6, 32-42.

Verhagen, M.M., Martin, J.J., van Deuren, M., Ceuterick-de Groote, C., Weemaes, C.M., Kremer, B.H., Taylor, M.A., Willemsen, M.A., Lammens, M., 2012. Neuropathology in classical and variant ataxia-telangiectasia. Neuropathology 32, 234-244.

Volkow, N.D., Tomasi, D., Wang, G.J., Studentsova, Y., Margus, B., Crawford, T.O., 2014. Brain glucose metabolism in adults with ataxia-telangiectasia and their asymptomatic relatives. Brain 137, 1753-1761.

Waldmann, T.A., McIntire, K.R., 1972. Serum-alpha-fetoprotein levels in patients with ataxia-telangiectasia. Lancet 2, 1112-1115.

Woods, C.G., Bundey, S.E., Taylor, A.M., 1990. Unusual features in the inheritance of ataxia telangiectasia. Hum Genet 84, 555-562.

Ying, S.H., Landman, B.A., Chowdhury, S., Sinofsky, A.H., Gambini, A., Mori, S., Zee, D.S., Prince, J.L., 2009. Orthogonal diffusion-weighted MRI measures distinguish region-specific degeneration in cerebellar ataxia subtypes. J Neurol 256, 1939-1942.

Yoon, B., Kim, J.S., Lee, K.S., Kim, B.S., Chung, S.R., Kim, Y.I., 2006. Early pathological changes in the cerebellum of patients with pure cerebellar syndrome demonstrated by diffusion-tensor imaging. Eur Neurol 56, 166-171.

Authors' Roles

Key: 1. Research project: A. Conception, B. Organization, C. Execution; 2. Statistical Analysis: A. Design, B. Execution, C. Review and

Critique; 3. Manuscript Preparation: A. Writing of the first draft, B. Review and Critique

Ishani Sahama: 1C, 2B, 2C, 3A, 3B.

Kate Sinclair: 1A, 1B, 3B

Simona Fiori: 2B, 2C, 3B.

James Doecke: 2B, 2C, 3B.

Kerstin Pannek: 2C, 3B.

Lee Reid: 2A, 2C, 3B.

Martin Lavin: 1A, 1B, 3B.

Stephen Rose: 1A, 1B, 1C, 2A, 2C, 3B.

Financial Disclosures of all authors

The funding for this project is from the A-T Children's Project (USA) and BrAshA-T (Australia). The authors of this manuscript have no other financial interest to disclose. Funding bodies were not involved in the drafting of this article unless otherwise stated under Author Roles or Acknowledgements.

Stock Ownership in medically-related fields: None.

Consultancies: None.

Advisory Boards: Human Ethics Institutional Review Board.

Partnerships: A-T Children's Project (USA) and BrAshA-T (Australia).

Honoraria: None.

Grants: A-T Children's Project (USA) and BrAshA-T (Australia).

Intellectual Property Rights: None.

Expert Testimony: None.

Employment: None.

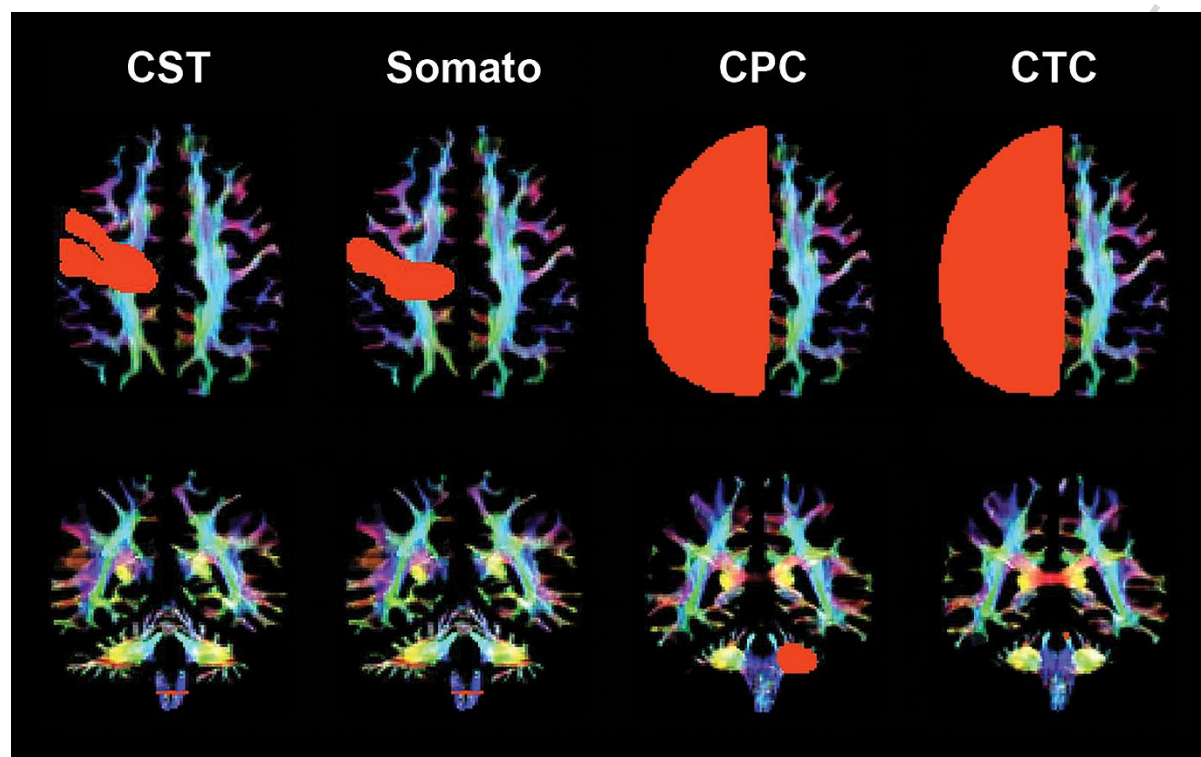**Contracts:** None.

Royalties: None.

Fig. 1. Region of Interest (ROI) placement for representative somatosensory motor cortex tracts for a control participant (age 23): Corticospinal (CST), somatosensory (Somato), cortico-ponto-cerebellar (CPC) and cerebellar-thalamo-cortical (CTC) tract ROIs in the cerebral cortex (first row) and cerebellar peduncles (second row). Colouration is based on the direction of water diffusion (Blue: ascending-descending diffusion; Red: Left-Right diffusion; Green: anterior-posterior diffusion).
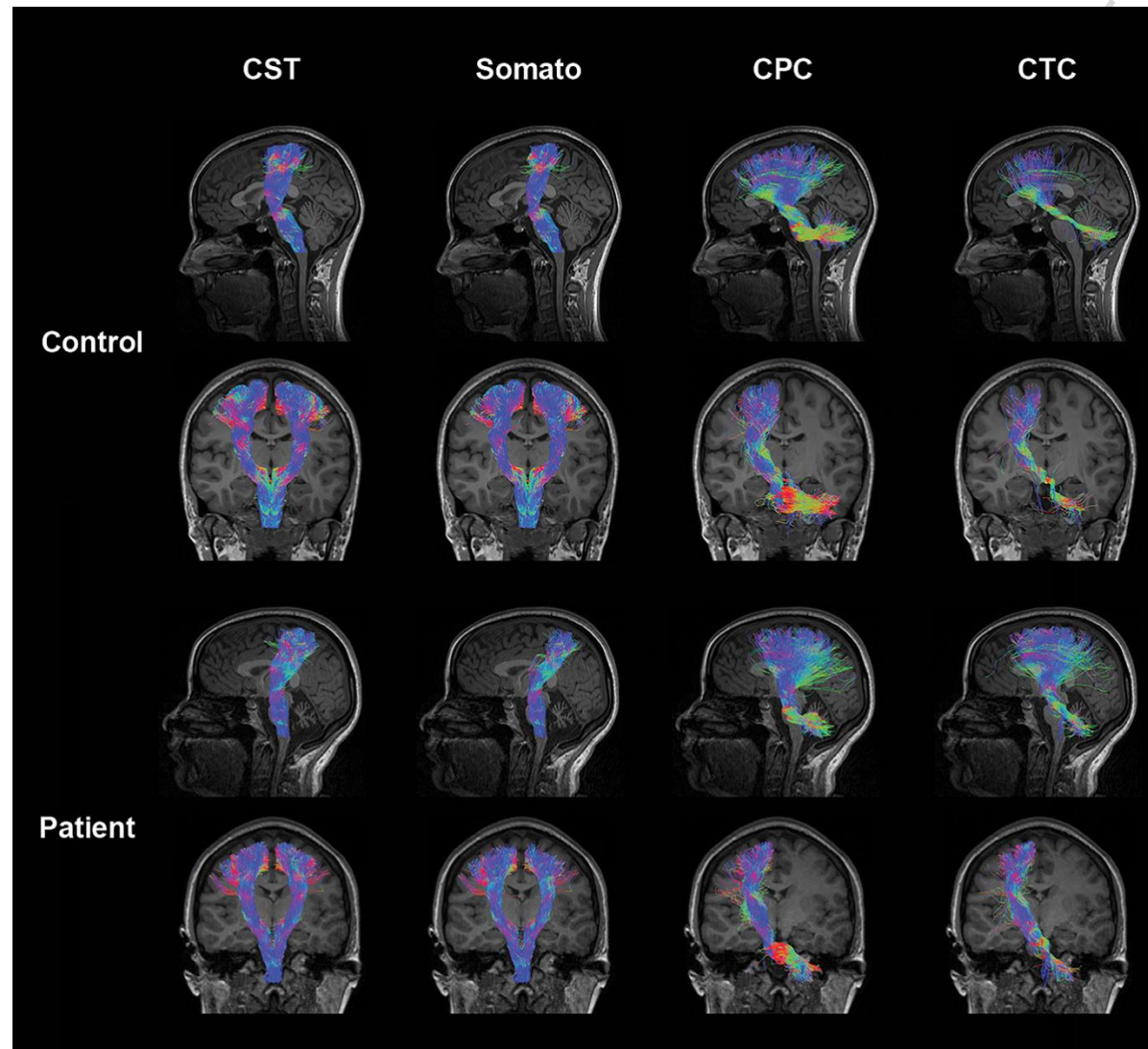
Fig. 2. Somatosensory motor tracts in a representative control and ataxia telangiectasia (A-T) subject (age 23): Control tracts are displayed in the first and second rows comprising the left sagittal (first row) tracts, left and right coronal (second row) corticospinal (CST) and somatosensory tracts, and left coronal (second row) cortico-ponto-cerebellar (CPC) and cerebellar-thalamo-cortical (CTC) tracts. Patient tracts are displayed in the third and fourth rows comprising the left sagittal (third row) tracts, left and right coronal (fourth row) CST and somatosensory tracts, and left coronal (fourth row) CPC and CTC tracts. Colouration of tracts is based on the direction of water diffusion (Blue: ascending-descending diffusion; Red: Left-Right diffusion; Green: anterior-posterior diffusion).
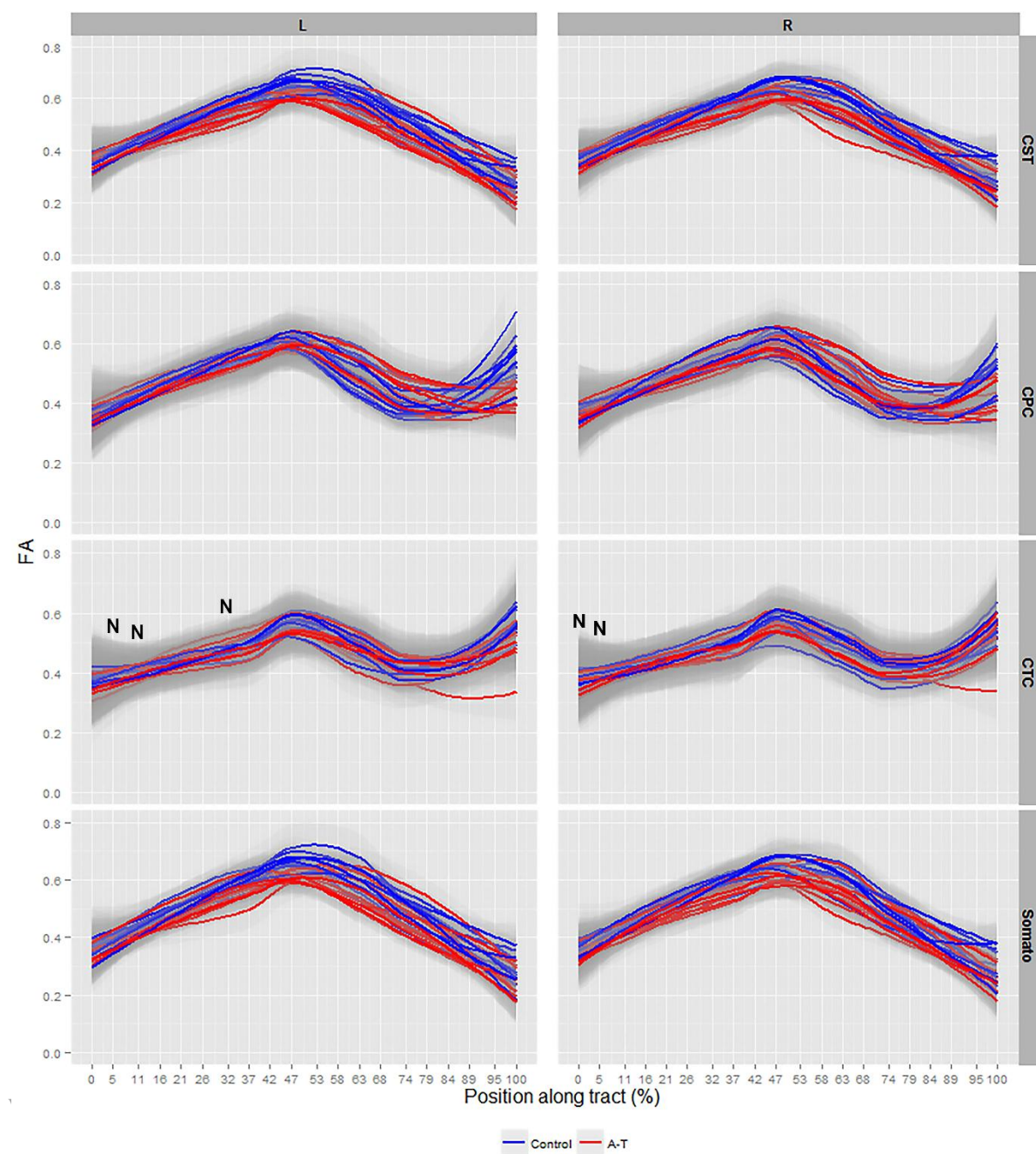
Fig. 3. Smooth estimates of the average fractional anisotropy (FA) of all controls (blue) and patients (red) are plotted versus position from tract origin (cerebral motor cortex (0%) – cerebellar peduncles (100%)), faceted by tract name (Corticospinal (CST), somatosensory (Somato), Cortico-ponto-cerebellar (CPC), Cerebellar-thalamo-cortical (CTC)) and hemisphere (Left (L.) and Right (R.) ± pointwise 99% confidence range (light gray shading)). Tract position at 0-5% represents precentral and postcentral gyrus layers, at 47-58% represents thalamic layers in all tracts and at 95-100% represents the spinal cord in CST and somatosensory tracts, and position of the medial cerebellar and superior cerebellar peduncles connecting the brainstem and cerebellum for the CPC and CTC tracts respectively. 'N' denotes tract locations with non-significant values.
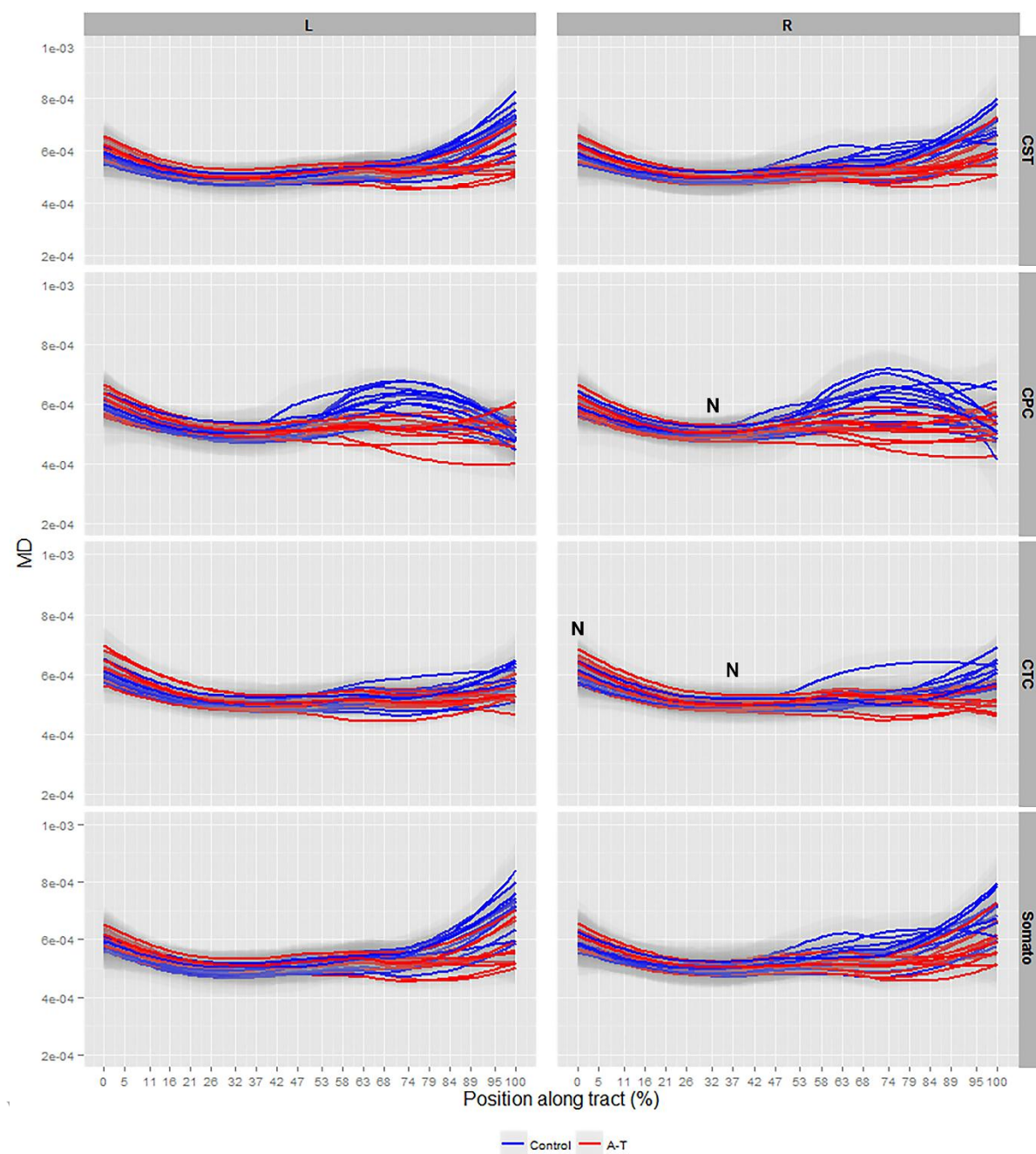
Fig. 4. Smooth estimates of the average mean diffusivity (MD) of all controls (blue) and patients (red) are plotted versus position from tract origin (cerebral motor cortex (0%) – cerebellar peduncles (100%)), faceted by tract name (Corticospinal (CST), somatosensory (Somato), Cortico-ponto-cerebellar (CPC), Cerebellar-thalamo-cortical (CTC)) and hemisphere (Left (L.) and Right (R.) ± pointwise 99% confidence range (light gray shading)). Tract position at 0-5% represents precentral and postcentral gyrus layers, at 47-58% represents thalamic layers in all tracts and at 95-100% represents the spinal cord in CST and somatosensory tracts, and position of the medial cerebellar and superior cerebellar peduncles connecting the brainstem and cerebellum for the CPC and CTC tracts respectively. 'N' denotes tract locations with non-significant values.
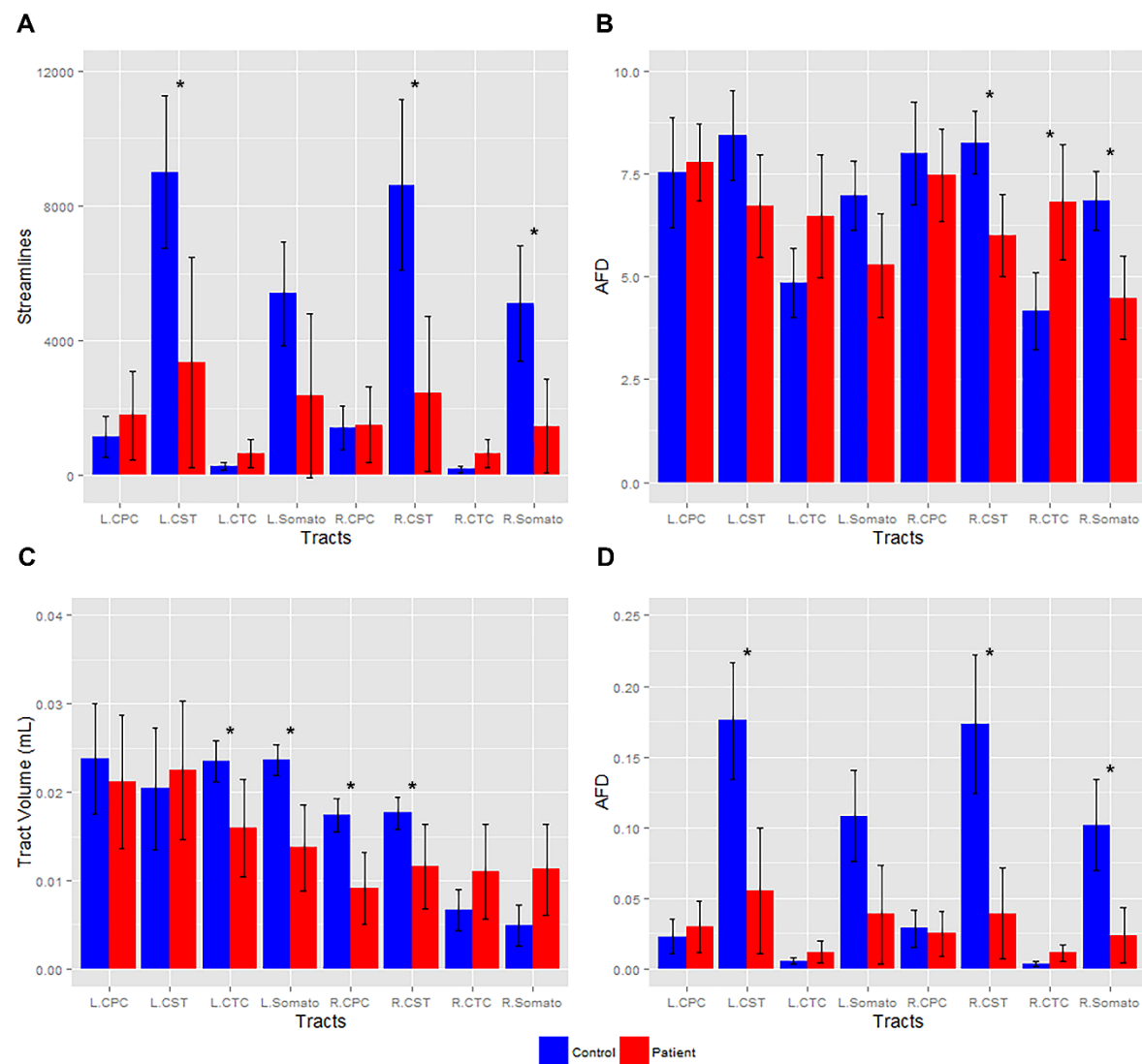
Fig. 5. Number of white matter (WM) streamlines, tract volume and apparent fiber density (AFD) in control and patient tracts: A) Mean number of streamlines in WM tracts (Corticospinal (CST), somatosensory (Somato), Cortico-ponto-cerebellar (CPC), Cerebellar-thalamo-cortical (CTC)) (Left (L.) and Right (R.) ± pointwise 95% confidence interval) is plotted with significance (*, $p < 0.006$). B) The mean AFD in WM tracts (Left (L.) and Right (R.) ± pointwise 95% confidence interval) is plotted with significance (*, $p < 0.006$). C) The mean tract volume (mL) in WM tracts (Left (L.) and Right (R.) ± pointwise 95% confidence interval) is plotted with significance (*, $p < 0.006$). D) The mean AFD in WM tracts (Left (L.) and Right (R.) ± pointwise 95% confidence interval) corrected for partial volume effects is plotted with significance (*, $p < 0.006$).